Kinetics and percolation: coke in heterogeneous catalysts

OPEN ACCESS
IOP Publishing
Journal of Physics A: Mathematical and Theoretical
J. Phys. A: Math. Theor. **55** (2022) 174005 (16pp)
https://doi.org/10.1088/1751-8121/ac5d81

Kinetics and percolation: coke in heterogeneous catalysts

Vladimir P Zhdanov*

Department of Physics, Chalmers University of Technology, Göteborg, Sweden
Boreskov Institute of Catalysis, Russian Academy of Sciences, Novosibirsk, Russia

E-mail: zhdanov@chalmers.se

Received 26 September 2021, revised 5 March 2022
Accepted for publication 14 March 2022
Published 31 March 2022

Abstract

In the conventional lattice percolation models, bonds or sites are open at random, whereas in reality there is often interplay of percolation and the kinetics under consideration. An interesting and practically important example is hydrocarbon conversion occurring in a reactor containing $\sim$1 mm-sized porous pellets with catalytic nanoparticles deposited at walls of the nanopores. Such catalytic heterogeneous reactions are often accompanied by coke formation deactivating catalytic nanoparticles and blocking pores for reactant diffusion, so that one needs to remove coke from time to time e.g. via reaction with oxygen. Herein, I first present generic coarse-grained Monte Carlo simulations of coke formation in a single pellet with the emphasis on the reaction regime influenced by reactant diffusion in pores. Then, the obtained coke distributions are used for similar simulations of coke removal. This combination of the models has allowed me to illustrate qualitatively new spatio-temporal regimes of the processes under consideration. For example, the removal of coke can be slow in the beginning, due to blocking of oxygen diffusion near the external pellet-gas interface and preventing its penetration to the central part of a pellet, and then fast when the pathways for diffusion to the center become to be open.

Keywords: Monte Carlo simulations, lattice models, percolation, heterogeneous catalysis, deactivation, regeneration, coke

(Some figures may appear in colour only in the online journal)

*Author to whom any correspondence should be addressed.

1. Introduction

The conventional lattice percolation models imply that bonds or sites are open with certain probability p which is considered to be a governing parameter [1, 2]. The percolation probability P is defined for lattices of large size (in the limit $L \to \infty$) as the probability that a single site or bond is connected with infinite number of other sites or bonds via open pathways. With increasing p, there is a critical threshold, p_c, at which the infinite percolation cluster makes its first appearance so that $P > 0$. During the past two decades, this classical percolation concept has been expanded in various directions (see e.g. [3] and references therein). One of them includes introduction of more complex (e.g., off-lattice) models and/or general rules for generation of open links as e.g. in continuum, explosive, and gradient percolation (see e.g. [4, 5] and references therein). Another general direction with numerous potential applications is associated with the studies of various physical, chemical, or biological spatio-temporal kinetic processes where percolation appears or disappears locally and then appreciably influences kinetics, i.e., there is interplay of kinetics and percolation. For example, fluid flowing through porous media may carry small solid particles which may attach to the walls and change the permeability of the medium, and then these changes may in turn influence percolation and deposition behaviors as a negative feedback [6]. Among more specific applications of current interest, one can refer to the percolation models aimed at various aspects of COVID-19 (see e.g. [7, 8]).

Spatio-temporal kinetic processes are abundant in chemistry in general and heterogeneous catalysis in particular. From the perspective of applications, heterogeneous catalysis with reactions occurring in reactors containing mm-sized porous pellets with catalytic nanoparticles (CNPs) deposited at walls of the pores is widely considered to be the most or at least one of the most important branches of chemistry, because it is inherent for the large-scale chemical industry [9, 10]. In particular, $\sim$80% of all chemical industrial processes includes heterogeneous catalysis, and it contributes directly or indirectly to $\sim$35% of the world's GDP [11]. In the context of basic studies, heterogeneous catalytic reactions (HCRs) occurring at the gas- or liquid-support interface are especially interesting due to their complexity related to lateral adsorbate–adsorbate interaction, surface heterogeneity, and spontaneous and adsorbate-induced surface restructuring (reviewed e.g. in [12–14]), especially in the practically important case of supported CNPs (reviewed e.g. in [15, 16]). Under such conditions, the applicability of the analytical models based on the mean-field kinetic equations introduced by analogy with the mass-action law for the gas-phase reactions is limited. The applicability of the simplest MC lattice-gas models is limited as well. All these complications make, however, the kinetics of HCRs much richer and physically more interesting. Nowadays, the analytical and MC approaches to describing the kinetics of HCRs are well developed [12–17] and the corresponding studies often benefit from the use of the *ab initio* methods (e.g. DFT) in order to characterize the energetics of HCRs [15, 18, 19].

One of the important and challenging problems in heterogeneous catalysis is catalyst deactivation. It may occur via poisoning of CNPs by adsorption of impurities from the feed stream [9], sintering or, more specifically, Ostwald ripening and/or agglomeration of CNPs [9, 20], or actual loss of catalytic species [9]. In reactions occurring with participation of hydrocarbons, the catalyst deactivation is often related to the formation of coke which not only reduces the activity of CNPs but also blocks the reactant supply via pores [9, 21], so that many catalysts need regeneration by burning off coke via reaction with oxygen [22]. The coke formation

and removal are complex processes representing interesting examples of the already mentioned interplay between kinetics and percolation, or, more specifically, between reaction and percolation.

2. Specifics of coke formation and removal

Typically, the length scale of catalytic reactors is ∼cm in laboratory experiments and ∼m in industrial systems [10]. In applications, CNPs are usually located in porous pellets (with the length scale of ∼mm) at the walls of pores. The fine structure of pellets and size of pores are diverse. There are regular (e.g., zeolites), amorphous mesoporous, and hierarchical porous structures (reviewed in [23]). Almost all mesoporous materials often used in industrial heterogeneous catalysis (e.g., silica, alumina, zirconia, or ceria) are amorphous [23]. The size distribution of pores in such catalysts is often bimodal including nanopores, 4–10 nm, and pores of larger sizes up to ∼10 μm [23, 24]. Physically, this means that a pellet can be viewed as an array of heterogeneous nanoporous (4–10 nm) regions of ∼30 μm size which are interconnected and partly separated by large pores (with size up to ∼10 μm). The total surface area of nanopores is much larger than that of large pores, and accordingly the catalysis occurs primarily at CNPs located at the walls of nanopores.

In applications, catalytic reactors typically operate at steady-state conditions. This means that the consumption of reactants during catalytic reaction inside pores is counterbalanced by reactant diffusion in pores. This balance can result in the appearance of the gradients in reactant concentration on different length scales. To scrutinize various scenarios of this interplay, one needs to know how the coefficient of reactant diffusion in porous media depends on their structure in general and on the pore-size distribution in particular. The corresponding experimental and theoretical studies are numerous (reviewed in [25]). For bimodal mesoporous materials used in catalysis, accurate models are still lacking. By analogy with the diffusion in solids with grains (reviewed in [26]), one of the ways to interpret reactant diffusion in this case is to use the simplest additive expression for the effective diffusion coefficient,

$$D_{\rm eff} = D_{\rm l} f + D_{\rm n}(1 - f), \tag{1}$$

where $D_{\rm n}$ and $D_{\rm l}$ are the coefficients of diffusion in nanopores and large pores, respectively, and f is the volume fraction of the latter pores. Taking into account that $f \ll 1$, the ratio of the two contributions to $D_{\rm eff}$ is $D_{\rm l} f/D_{\rm n}$. In large pores, diffusion is molecular; whereas in nanopores, diffusion is often of the Knudsen type, and accordingly $D_{\rm l} \gg D_{\rm n}$. Thus, the ratio $D_{\rm l} f/D_{\rm n}$ can be in a wide range. With this reservation, this ratio is usually considered to be small so that the diffusion is controlled by nanopores.

At the level of pellets, the role of reactant diffusion in catalytic reactions is characterized by the effectiveness factor defined as the ratio of the average reaction rate to the rate calculated in the limit when the diffusion limitations are negligible. For the simplest first-order reaction running in a spherical pellet of radius R in the absence of complicating factors (such as coke), the text-book Thiele expressions for the reactant concentration and the effectiveness factor are [27]

$$\frac{c(r)}{c(R)} = \frac{R\,\sinh(r/\lambda)}{r\,\sinh(R/\lambda)} \quad \text{and} \quad \eta = \frac{3}{\phi}\left[\frac{\cosh\,\phi}{\sinh\,\phi} - \frac{1}{\phi}\right], \tag{2}$$

where r is the radial coordinate, $\lambda \equiv (D_{\rm eff}/k_{\rm eff})^{1/2}$ is the scale of the diffusion length ($k_{\rm eff}$ is the effective reaction rate constant), and $\phi = (k_{\rm eff}R^2/D_{\rm eff})^{1/2}$ is the corresponding modulus. A similar expression for η is available for cylindrically shaped pellets. In other cases, η should

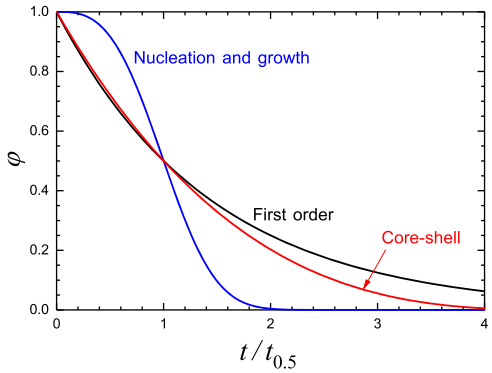

Figure 1. Fraction of the pore space filled by coke as a function of normalized time ($t_{0.5}$ corresponds to $\varphi = 0.5$) during coke removal according to the first-order model (equation (3)), shrinking-core model (equation (4)), and nucleation and growth model (equation (5)).

usually be calculated numerically (see e.g. [28]). In fact, expression (2) for η can be used for estimates in various situations provided R is identified with the scale of the pellet size (below, R can be identified with $L/2$). In the case of rapid diffusion ($\phi \ll 1$), the reactant distribution in pellets is nearly uniform so that $\eta \simeq 1$. In the case of slow diffusion ($\phi \gg 1$), the reactant concentration is relatively high near the external pellet-gas interface and drops inside so that $\eta \simeq 3/\phi \ll 1$. In fact, η characterizes percolation of a pellet by reactant in the context of the interplay of diffusion and reaction. The difference between η and the conventional percolation probability, P, is that the former always tends to zero with increasing the lattice size.

The formation and subsequent removal of coke take place primarily in nanopores. Chemically, the coke formation accompanying catalytic conversion of hydrocarbons represents a complex polymerisation reaction, whereas the coke removal can be viewed as a burn-off reaction occurring with participation of oxygen [21, 29]. In industrial reactors, both these processes depend on the spatio-temporal interplay of reaction itself, reactant diffusion, and coke formation or removal on all the length scales mentioned above, and the complete analysis of the kinetics of these processes should be done at the level of a whole reactor. The corresponding calculations are now available only for models with highly simplified reactant transport (see, e.g., [22, 30]). For more complex models, as usual, one should first clarify what may happen inside a porous pellet provided the reactant concentrations at the external pellet-gas interface are fixed. This is discussed and simulated below.

The rate of the coke formation depends on the reactant distribution in pellets, and accordingly the coke-formation kinetics depend on whether the main reaction occurs in the kinetically or diffusion-limited regimes (with $\phi \ll 1$ or $\phi \gg 1$, respectively). One of the first analytical models allowing one to describe various reaction regimes implies that the carbon (or poison) deposition in a pellet results in formation of a core–shell structure with a catalytically inactive shell, so that the reactant diffuses through this shell, and the main reaction occurs in a shrinking catalytically active core (section 6.2.2.2 in [9]). In fact, this model is suitable for poisoning rather than for carbon formation because the latter process can occur not only at the core–shell interface. The first phenomenological kinetic models taking percolation during the coke formation more explicitly into account were proposed for the kinetically limited regime of the main reaction (reviewed, e.g., in [29, 31]). For example, one can view the free space in a porous solid as a set of relatively large nanovoids interconnected by relatively small nanonecks with

the corresponding size distributions, so that voids and necks form a three-dimensional (3D) network. Pore blockage can be assumed to be caused primarily by blockage of necks and to be described by introducing the time-dependent critical radius, $r_c(t)$ (with e.g. $r_c(t) = vt$ or $wt^{1/2}$, where v and w are the corresponding rate constants), so that the necks with $r < r_c(t)$ are either literally blocked by coke or not fully blocked by coke but associated with inaccessible clusters of voids. The main reaction can be considered to occur only in accessible clusters of voids. The fraction of necks with $r < r_c(t)$ can be calculated by using the neck-size distribution, and then the model can be formalized mathematically in terms of the conventional bond percolation theory [31].

In more recent theoretical studies, a pellet is represented as the 2D network of cylindrical pores and the main reaction and coke formation occurring in these pores are described analytically taking explicitly the reactant diffusion via each pore into account [32]. There are also recent studies based e.g. on (i) lattice Boltzmann simulations of multicomponent reaction–diffusion and coke formation in a catalyst with hierarchical pore structure [33], (ii) DFT-backed molecular dynamics method [34], and (iii) population balance theory [35]. Taken together, such models allow one to describe reactions running in various reaction regimes.

One could expect that the coke distribution in pellets, predicted by the kinetic models of the pore blockage by coke, would naturally be used as the initial condition for the kinetic models describing coke removal. This is, however, not the case. One of the reasons of this state of the art is that in the former models taking percolation into account the final coke distribution is complex and not described analytically, and accordingly its use in the latter models is far from straightforward. In fact, the latter models are now highly simplified. For example, the analysis of decoking process in reactors is often based on the analysis of O_2 transport in reactor including diffusion and coke removal in pellets, and the latter is described by using the reaction–diffusion equation with the first-order expression for the burn-off reaction rate and constant (coke-independent) $D_{\rm eff}$ [22, 30].

Under isothermal conditions with constant O_2 concentration in pores, the simplest temporal first-order equation for the fraction of the pore space filled by coke in a pellet is

$$\varphi = \exp(-kt), \tag{3}$$

where k is the lumped burn-off rate constant (including O_2 concentration). Other conventional kinetic models were used in this context as well [36, 37]. For example, one of the apparently relevant models implies that the coke removal in a spherical pellet occurs at the interface of the shrinking coke core, so that

$$\varphi = (1 - kt)^3. \tag{4}$$

Another conventional model is based on the assumption that the coke removal starts at randomly located centers and then the corresponding spherical reaction fronts move linearly, so that

$$\varphi = \exp(-kt^3). \tag{5}$$

The kinetics predicted by equations (3)–(5) are shown in figure 1.

Below, using the coarse-grained lattice-gas model, I first present generic kinetic MC simulations of the coke formation in a porous pellet with the emphasis on the case when the main reaction is influenced by diffusion (in terms of the Thiele modulus, this means that $\phi \simeq 1$ or $\phi \gg 1$). Then, the obtained coke distributions are used for similar simulations of the

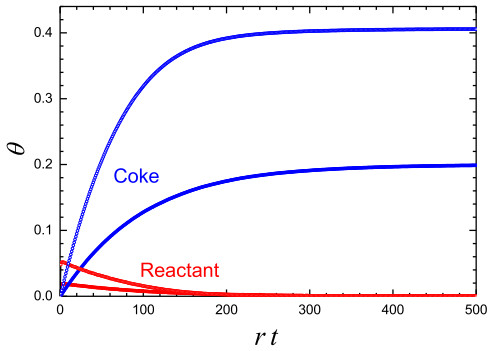

Figure 2. MC kinetics of coke formation in a 3D lattice with $L = 100$: fractions of sites occupied by reactant (R) and coke (C) are shown as a function of time for $r/k_{\rm tot} = 10^{-3}$ (open circles) and 10^{-2} (filled circles). Each kinetic curve exhibited here and below in figures 3, 5 and 8 was obtained by using one MC run. In all the cases, the fluctuations are fairly low because the number of lattice sites is large, 10^6.

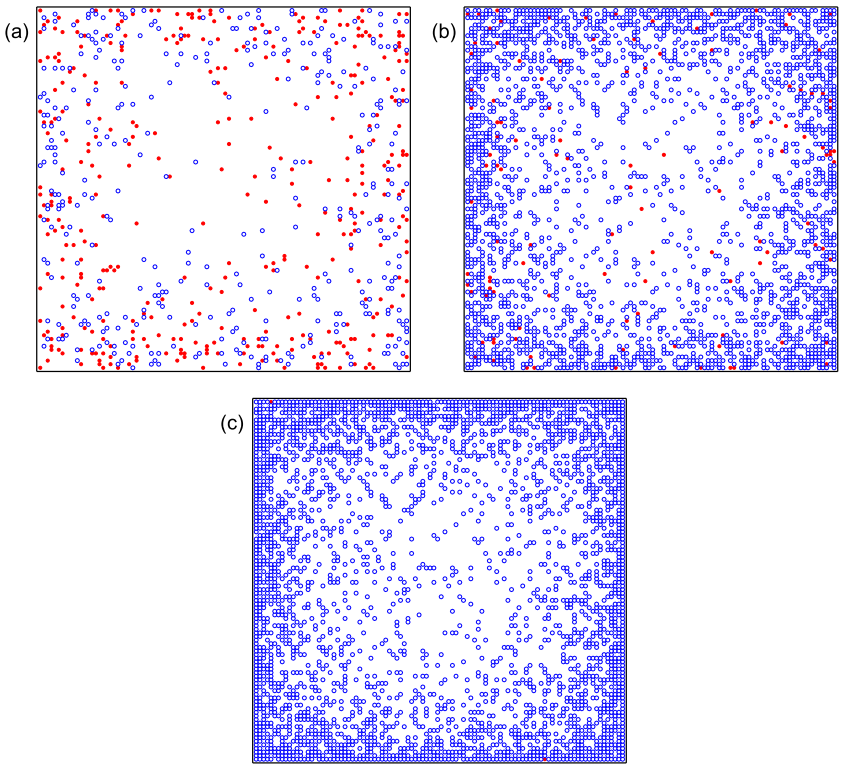

Figure 3. Snapshots of the 100×100 cross-section of the main $100 \times 100 \times 100$ lattice at its middle (along one of the directions) during the MC run with $r/k_{\rm tot} = 10^{-3}$ (figure 2, open circles) at $rt = 10$ (a), 100 (b), and 500 (c). Reactant, R, and coke, C, are shown by filled and open circles, respectively.

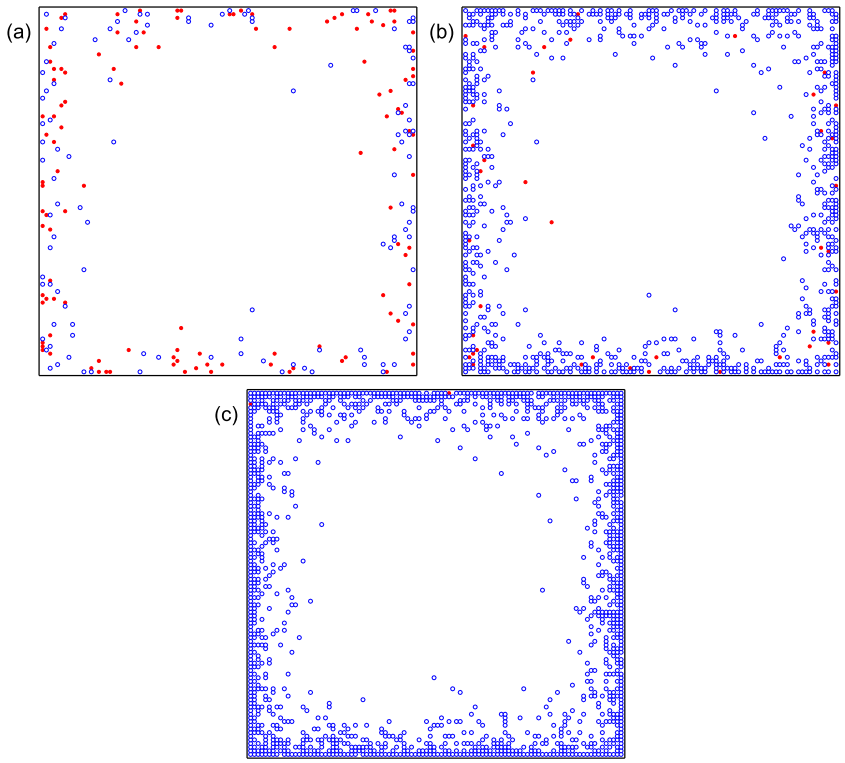

Figure 4. As figure 3 for the MC run with $r/k_{\rm tot} = 10^{-2}$ (figure 2, filled circles).

coke removal. Thus, both processes are described consistently. The corresponding MC algorithms take the specifics of the processes into account. Basically, the algorithms are similar and represent realization of one of the standard general algorithms for lattice MC simulations [38].

One of the key simplifications employed in the models is that the allowed diffusion jumps are considered to occur between the lattice sites with the same rate. Due to this simplification, the models can be qualitatively applicable to catalysts with the bimodal pore-size distribution provided the reactant diffusion is controlled by nanopores (4–10 nm) so that large pores are negligible. In the opposite less-probable regime when the reactant diffusion is globally controlled by large pores (with size up to $\sim$10 μm) partly separating heterogeneous regions (of $\sim$30 μm size) with nanopores, the models can be applicable to such regions. In reality, nanopores and larger pores can be important simultaneously. Theoretically, this case is interesting as well. The corresponding MC simulations are, however, beyond my current goals.

In principle, the models used below can be qualitatively applicable not only to coke formation and removal but also to other reactions occurring e.g. with formation of some immobile reaction product.

3. MC simulations of coke formation in a pellet

In the employed coarse-grained model, a porous pellet is represented by a cubic $L \times L \times L$ lattice (simulations for pellets of other e.g. spherical or cylindrical shapes can be performed by analogy, and it does not influence the main qualitative conclusions). Each lattice site forming

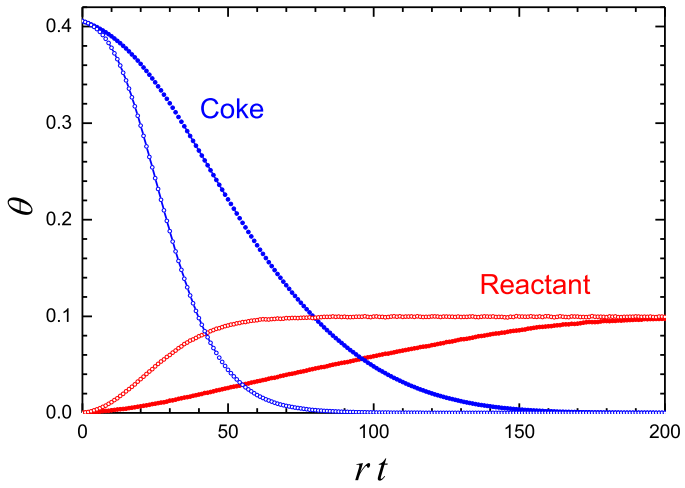

Figure 5. MC kinetics of coke removal in a 3D lattice with $L = 100$: fractions of sites occupied by reactant (R) and coke (C) are shown as a function of time for $r/k_{\rm tot} = 10^{-3}$ (open circles) and 10^{-2} (filled circles). The initial C distribution is with weak C gradients (as exhibited in figure 3(c)).

porous space can be vacant or occupied by a reactant, R (hydrocarbon), or coke, C. By analogy with the simplest Thiele model (equation (2)), the main first-order reaction is considered to result in disappearance of R,

$$\mathrm{R} \to \emptyset, \tag{6}$$

and the products of this reaction are not tracked. The coke formation is mimicked in a lumped way by the simplest first-order reaction as well,

$$\mathrm{R} \to \mathrm{C}. \tag{7}$$

R is allowed to diffuse via jumps to nearest-neighbour (nn) sites, whereas C is immobile. Initially (at $t = 0$), the $L \times L \times L$ lattice is considered to be free of R and C.

To mimic the R supply at the boundaries, the sites adjacent to the $L \times L \times L$ lattice (these sites mimic the gas phase outside a pellet) are considered to be partly occupied by R with the prescribed average coverage, $\theta_{\rm adj}$ (as in the grand-canonical distribution). Practically, this means that in simulation after selection such a site is considered to be vacant with probability $1 - \theta_{\rm adj}$ or occupied by R with probability $\theta_{\rm adj}$. The R jumps between adjacent sites and boundary sites of the $L \times L \times L$ lattice are considered to occur with the same rate as those inside the lattice. The rate constants of steps (6) and (7) and diffusion jumps are designated as $k_{\rm r}$, $k_{\rm c}$, and $k_{\rm d}$, respectively.

In this model, each site physically represents a void, and the main simplification is that a site can be in three discrete states (vacant or occupied by R or C). In reality, the main reaction and coke formation occur in a nanopores, and the latter process is continuous, i.e., includes many polymerization acts. Despite this difference, the model is physically reasonable as the simplest coarse-grained approximation and can be especially useful in order to scrutinize the interplay of the diffusion-limited reaction kinetics and coke-related percolation. This is the case because (i) the main reaction in the model represents the lattice version of the conventional first-order reaction (as in the Thiele model (equation (2))) and correctly describes the reactant distribution

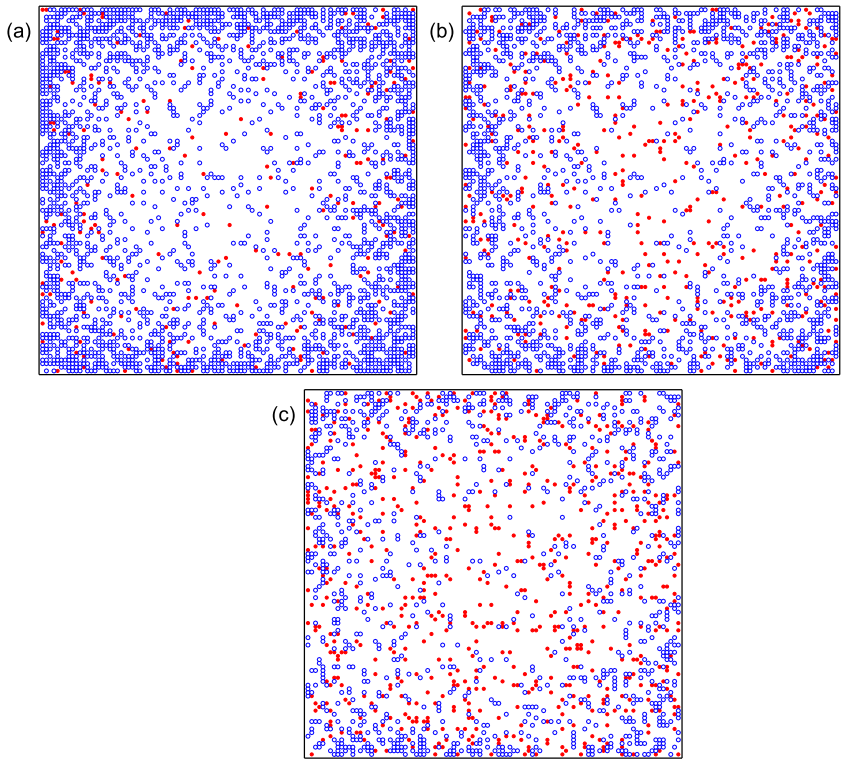

Figure 6. Snapshots of the 100×100 cross-section of the main $100 \times 100 \times 100$ lattice at its middle during the MC run with $r/k_{\rm tot} = 10^{-3}$ (figure 5, open circles) at $rt = 15$ (a), 25 (b), and 35 (c). Reactant, R, and coke, C, are shown by filled and open circles, respectively.

during the diffusion-influenced regimes, and (ii) the rate of the coke formation can in general be considered to be just proportional to the local reactant concentration and accordingly is in this case described correctly despite the discreteness of the site states. (The simplicity of this model and the model used below in section 4 is to some extent similar to that of the celebrated ZGB MC model [39].)

With the specification above, the MC simulations consist of sequential trials of realisation of one of possible events at one of the randomly chosen sites at the $(L+2) \times (L+2) \times (L+2)$ lattice (this lattice includes the main $L \times L \times L$ lattice and adjacent sites). In such simulations, one should use dimensionless probabilities of various kinetic steps. Such probabilities are introduced by dividing the rate constants of kinetic steps by suitably chosen rate constant, k_* which should be equal or larger that the sum of the specific rate constants [38]. The choice of k_* is not unique, and accordingly the introduction of the specific probabilities is not unique either. Often, the convenient choice of k_* is to set it equal to the sum of the specific rate constants, i.e., to $k_{\rm tot} = k_{\rm r} + k_{\rm c} + k_{\rm d}$ in the model under consideration. Following this line, I define the specific probabilities as the ratios of $k_{\rm r}$, $k_{\rm c}$, and $k_{\rm d}$ to $k_{\rm tot}$. Then, the algorithm I use is as follows:

(a) A site located on the whole (main + adjacent) lattice is chosen at random. If this site is on the main lattice, the following actions depend on its state and are performed as described

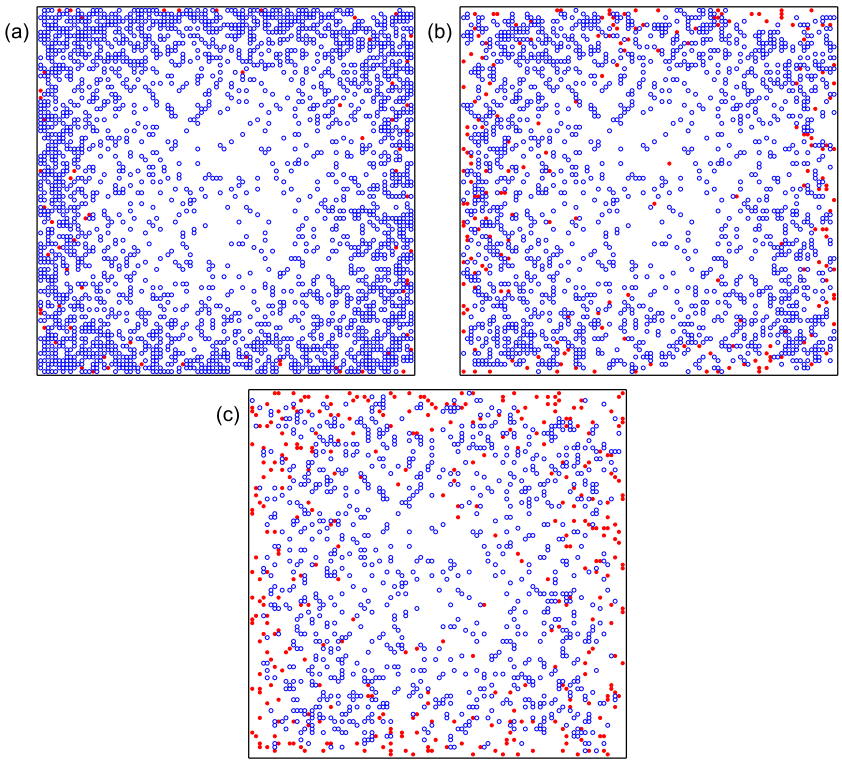

Figure 7. As figure 6 for the MC run with $r/k_{\rm tot} = 10^{-2}$ (figure 5, filled circles) at $rt = 25$ (a), 50 (b), and 75 (c).

in items (b), (c), and (e) below. If this site is on the adjacent lattice, it is considered to be vacant with probability $1 - \theta_{\rm adj}$ or occupied by R with probability $\theta_{\rm adj}$, and after identification of its state the following actions are performed as described in items (b), (d), and (e) below.

(b) If the site chosen is vacant or occupied by C, a trial ends.

(c) If the site selected belongs to the main lattice and is occupied by R, steps (6) and (7), or diffusion jump is realized with probabilities $k_{\rm r}/k_{\rm tot}$, $k_{\rm c}/k_{\rm tot}$, and $k_{\rm d}/k_{\rm tot}$. For diffusion, one of the nn sites is chosen at random and the jump is performed provided the latter site is vacant.

(d) If the site selected is adjacent to the main lattice and occupied by R, the diffusion jump is realized with probability $k_{\rm d}/k_{\rm tot}$ as described in (c).

(e) After each MC trial, the dimensionless MC time is incremented by $\Delta t_{\rm MC} = |\ln(\rho)|/(L+2)^3$, where $0 < \rho \leqslant 1$ is a random number. (The use of $|\ln(\rho)|$ is related to the fact that each kinetic event represents a Poisson process.)

On average, we have $\langle|\ln(\rho)|\rangle = 1$, and accordingly $\Delta t_{\rm MC} = 1$ corresponds to $(L+2)^3$ MC trials. In the present simulations, as usual, $\Delta t_{\rm MC} = 1$ is identified with one MC step. To convert $t_{\rm MC}$ into real time, t, it should be divided by $k_{\rm tot}$. Real time is needed if a model is used to describe/fit real kinetics. My goal is rather to show theoretically general trends in the kinetics. In the latter case, it is convenient to multiply t by a suitably chosen rate constant. One of the options which is often employed is to multiply t by $k_{\rm tot}$, i.e., to use $t_{\rm MC}$. In the simulations

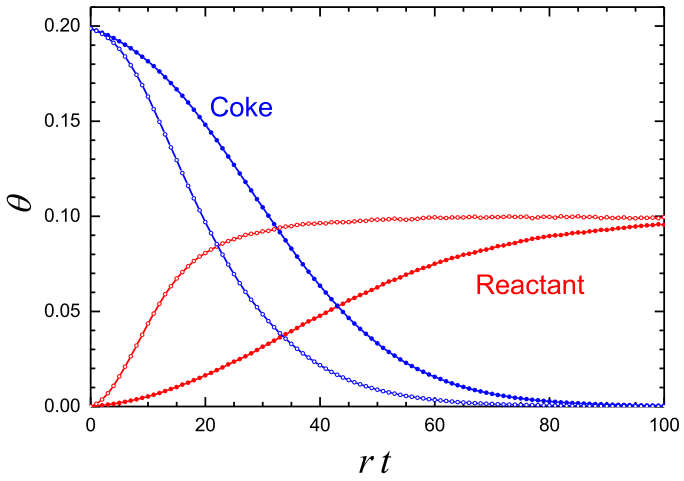

Figure 8. MC kinetics of coke removal in a 3D lattice with $L = 100$: fractions of sites occupied by reactant (R) and coke (C) are shown as a function of time for $r/k_{\rm tot} = 10^{-3}$ (open circles) and 10^{-2} (filled circles). The initial C distribution is with appreciable C gradients (as exhibited in figure 4(c)).

presented below, the diffusion is fast compared to reaction steps (6) and (7) (this limit is expected to correspond to reality), and $t_{\rm MC}$ is related primarily to diffusion. In chemistry, the dimensionless time is, however, customarily associated with reactions. Following this line, I introduce the rate constant $r = k_{\rm r} + k_{\rm c}$ characterizing steps (6) and (7) and use $rt \equiv rt_{\rm MC}/k_{\rm tot}$ as the dimensionless time in order to exhibit the results.

MC runs were performed on a 3D lattice with $L = 100$ and $\theta_{\rm adj} = 0.1$. As already mentioned, the main lattice was initially (at $t = 0$) free of R and C. The main reaction (with $k_{\rm r}/r = 0.9$) was appreciably faster than the coke formation (with $k_{\rm c}/r = 0.1$) and much slower (3 or 2 orders of magnitude) than R diffusion.

Typical MC kinetics of the coke formation or, more specifically, fractions of sites occupied by R and C are shown in figure 2. In terms of the percolation theory, the latter fraction characterizes, in a lumped way, blocking the lattice sites. The former fraction divided by $\theta_{\rm adj}$ characterizes, also in a lumped way, accessibility of sites. Thus, basically, such kinetics characterize the loss of percolation of a pellet by reactant in the context of the interplay of diffusion, reaction, and coke formation.

The kinetics exhibited (figure 2) were calculated with $r/k_{\rm tot} = 10^{-3}$ and 10^{-2}. In both these cases, the kinetics are apparently simple. In particular, the R and C concentration monotonously decreases and increases, respectively. The percolation threshold is not well manifested. The effect of percolation on the kinetics is, however, appreciable in both cases and especially for slower R diffusion (with $r/k_{\rm tot} = 10^{-2}$). This is manifested in the fact that only a part of the lattice sites (0.40 for $r/k_{\rm tot} = 10^{-3}$ and 0.20 for $r/k_{\rm tot} = 10^{-2}$) is filled by C in the end.

Typical lattice snapshots for the kinetics with faster R diffusion ($r/k_{\rm tot} = 10^{-3}$) are shown in figure 3. In terms of the Thiele modulus (equation (2)), $r/k_{\rm tot} = 10^{-3}$ corresponds to $\phi \simeq 1$. This means that the regime of the main reaction is between kinetically and diffusion-limited. In this case, the gradients in the R and C concentration are nearly negligible in the beginning (figure 3(a)). In the end, the gradients in the C concentration are observed on the length scale comparable with the lattice size (figure 3(c)).

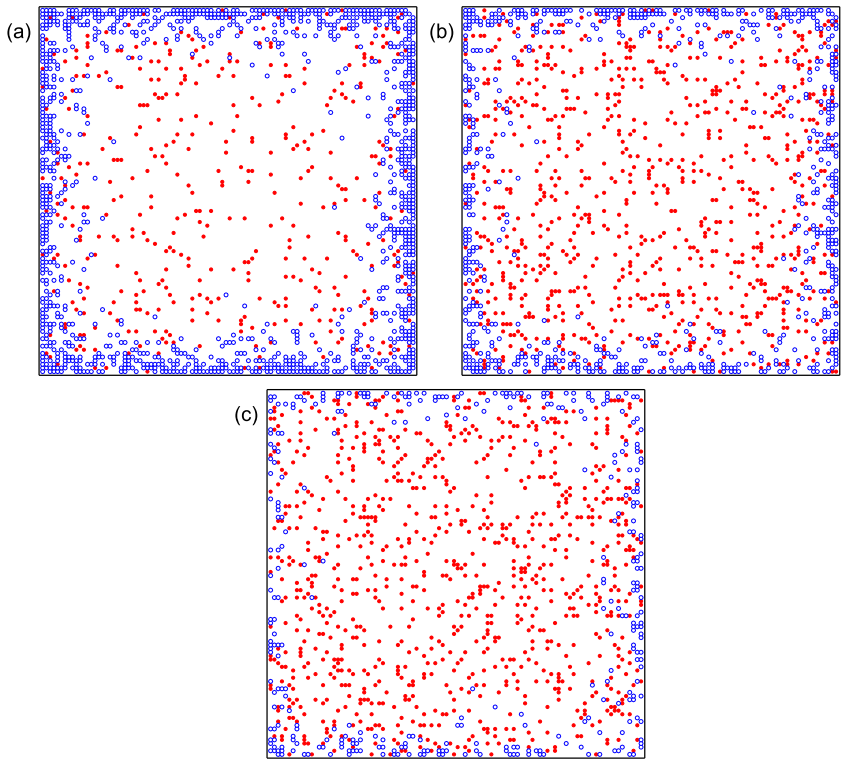

Figure 9. Snapshots of the 100×100 cross-section of the main $100 \times 100 \times 100$ lattice at its middle during the MC run with $r/k_{\rm tot} = 10^{-3}$ (figure 8, open circles) at $rt = 10$ (a), 20 (b), and 30 (c). Reactant, R, and coke, C, are shown by filled and open circles, respectively.

Typical lattice snapshots for the kinetics with slower R diffusion ($r/k_{\rm tot} = 10^{-2}$) are exhibited in figure 4. In this case, $r/k_{\rm tot} = 10^{-2}$ corresponds to $\phi > 1$, and accordingly the main reaction occurs in the diffusion-limited regime. In this case, R and C are distributed primarily near the lattice boundary.

In the absence of coke, the reactant distributions shown in figures 3 and 4 for a cubically shaped pellet are qualitatively similar to those predicted analytically (equation (2)) for a spherical pellet. The analytical expression for the reactant distribution in a cubically shaped pellet (as in the model under consideration) can be obtained as well, but it is cumbersome and not instructive. In the presence of coke, the corresponding analytical expressions are lacking.

4. MC simulations of coke removal in a pellet

As noticed in section 2, one of the goals of my work was to perform consistent simulations of coke formation and removal. Following this line, I used the C distributions obtained in the end of the MC kinetics of coke formation (figures 3(c) and 4(c)) as the initial condition for simulations of coke removal. The latter process is represented as reaction between R (oxygen) and C located in the nn sites,

$$\mathrm{R} + \mathrm{C} \to \emptyset. \tag{8}$$

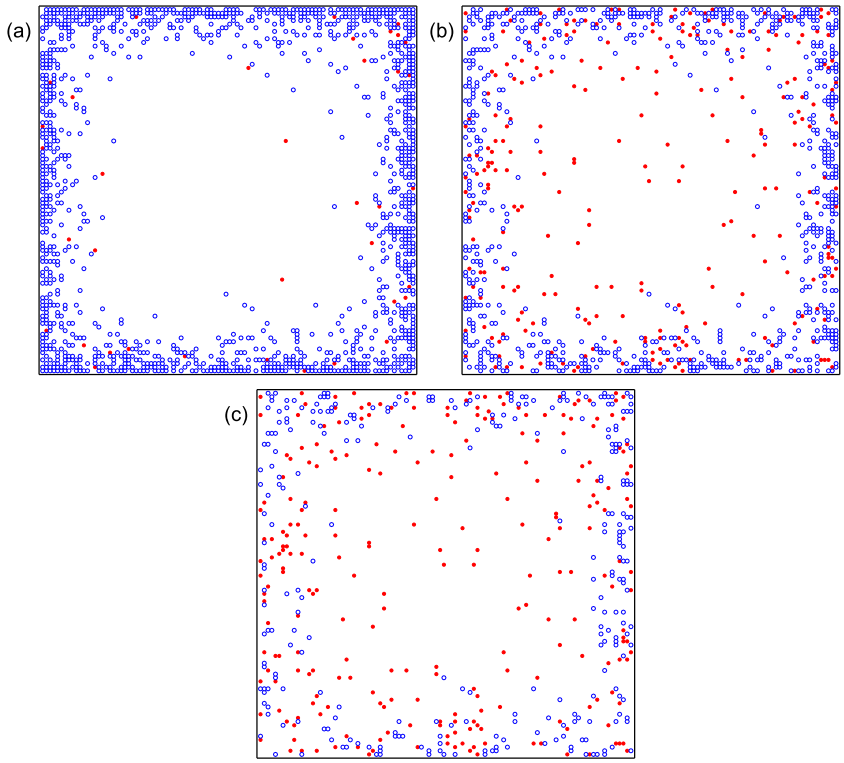

Figure 10. As figure 9 for the MC run with $r/k_{\rm tot} = 10^{-2}$ (figure 8, filled circles) at $rt = 10$ (a), 30 (b), and 50 (c).

The MC algorithm of these simulations was similar to that described in section 3. The only difference is that now there is no step (6) whereas step (7) is replaced by (8). The latter step is realized provided the site chosen is occupied by R. In such cases, one of the nn sites is selected at random, and if this site is occupied by C, step (8) is realized with probability $r/k_{\rm tot}$, where r is the rate constant corresponding to this step, and $k_{\rm tot} = r + k_{\rm d}$ is a sum of the two rate constants. The simulations were performed on the same lattice ($L = 100$) as in section 3 with similar kinetic parameters, $\theta_{\rm adj} = 0.1$ and $r/k_{\rm tot} = 10^{-3}$ and 10^{-2}.

Typical MC kinetics of the coke removal or, more specifically, fractions of sites occupied by R and C are presented in figures 5 and 8. As already noticed in section 3, the former fraction divided by $\theta_{\rm adj}$ characterizes accessibility of sites whereas the latter fraction characterizes blocking the lattice sites. Thus, such kinetics show restoration of percolation of a pellet via reactant diffusion and reaction with coke.

In particular, the kinetics calculated by using the initial C distribution with weak C gradients (figure 3(c)) are exhibited in figure 5. Examples of the lattice snapshots corresponding to the kinetics with the selected values of $r/k_{\rm tot}$ are shown in figures 6 and 7. In both cases, the dependence of the reaction timescale on R diffusion is rather weak (figure 5). The process is slow in the beginning as long as it occurs near the lattice boundary (figures 6(a) and 7(a)). Afterwards, after reducing C concentration near the lattice boundary and increasing R percolation to the central part of the lattice, the process becomes rapid (figures 6(b) and (c) and 7(b) and (c)).

For the initial C distribution with appreciable C gradients (figure 4(c)), the results are shown in figures 8–10. The corresponding kinetics calculated also with $r/k_{\rm tot} = 10^{-3}$ and 10^{-2} (figure 8) are qualitatively similar to those exhibited in figure 5. Examples of the lattice snapshots illustrating these kinetics are given in figures 9 and 10.

5. Conclusion

The studies of percolation occurring in the course of various physical, chemical, or biological spatio-temporal kinetic processes are just beginning. Herein, I have presented generic coarse-grained MC simulations of two processes of this category. The first one is coke formation in the course of heterogeneous catalytic reaction running in a porous pellet with the emphasis on the case when this reaction is influenced by reactant diffusion in pores. The obtained coke distributions were used for similar simulations of burning off coke via reaction with oxygen.

Despite its simplicity, the model employed for coke formation is different compared or at least not fully identical to the already available models (briefly reviewed in section 2). Thus, the results obtained in the framework of this model are complementary to those published earlier. The diversity of models in this area is a consequence of the complexity of the process under consideration.

In the context of the experimental and theoretical studies (briefly reviewed in section 2), the current simulations of the coke removal are most interesting, because in the earlier studies this process was described by employing the first-order model [22, 30] or other phenomenological analytical models based on the assumption that initially the coke distribution in a pellet is uniform or that all the porous space is fully filled by coke [36, 37]. These models are not applicable in the cases when the main reaction inducing the coke formation is influenced or limited by reactant diffusion so that the final coke distribution is not uniform (section 3), and accordingly the initial coke distribution in the process of catalyst regeneration is not uniform either (section 4). Such regimes are common in practice. The MC simulation presented (section 4) show the specifics of the spatio-temporal kinetics in this case. In particular, the removal of coke is predicted to be slow in the beginning, due to blocking of oxygen diffusion near the external pellet-gas interface and preventing its penetration to the central part of a pellet, and then to be fast when the pathways for diffusion to the center become to be open. These kinetics are apparently similar to those predicted by two conventional phenomenological models. One of them is the classical nucleation and growth model (equation (5) and figure 1). Another more formal model is based on the axiomatic description of the kinetics by using the temporal power-low equation, $\mathrm{d}\varphi/\mathrm{d}t = -k(1-\varphi)^n$, with $n > 0$. Physically, however, these conventional phenomenological models and the MC model under consideration are completely different. Taken together, the results presented (especially those shown in section 4) help to form the conceptual basis in the area under consideration. The identification of the predicted kinetic features (section 4) in experiments is now not straightforward because the initial distribution of coke in reactions influencing by diffusion is still poorly characterized.

Finally, I can articulate that the model employed is qualitatively applicable to pellets with the bimodal pore-size distribution provided the reactant diffusion is controlled by nanopores (4–10 nm). If the reactant diffusion in a pellet is globally controlled by large pores (with size up to $\sim$10 μm) partly separating heterogeneous regions (of $\sim$30 μm size) with nanopores, the model can be applicable to such regions. In the latter case, the apparent kinetics of coke formation and removal can be appreciably influenced by the distribution of sizes of these regions (by analogy e.g. with oxidation of nm-sized soot spherules [40]). The model does not, however, describe the interplay of diffusion via nanopores and large pores. This interplay can be important even if the reactant diffusion in a pellet during the main reaction in the absence of coke is

controlled by nanopores. If these pores are blocked by coke near the external pellet-gas interface, the large pores may be still operative. The corresponding channel of reactant diffusion towards the center of a pellet can be slow, but at the long timescale it can appreciably influence the coke distribution in a pellet. The subsequent kinetics of coke removal will be influenced as well. Such effects merit attention and are expected to be scrutinized in the nearest future both experimentally and theoretically.

Acknowledgments

This work was supported by Ministry of Science and Higher Education of the Russian Federation within the governmental order for Boreskov Institute of Catalysis (project AAAA-A21-121011390008-4). The author thanks Dr A N Zagoruiko for useful communication.

Data availability statement

All data that support the findings of this study are included within the article (and any supplementary files).

ORCID iDs

Vladimir P Zhdanov https://orcid.org/0000-0002-0167-8783

References

[1] Stauffer D and Aharony A 1994 *Introduction to Percolation Theory* 2nd edn (London: Taylor and Francis)
[2] Newman M E J and Ziff R M 2000 Efficient Monte Carlo algorithm and high-precision results for percolation *Phys. Rev. Lett.* **85** 4104–7
[3] Xun Z, Hao D and Ziff R M 2022 Site and bond percolation thresholds on regular lattices with compact extended-range neighborhoods in two and three dimensions *Phys. Rev.* E **105** 024105
[4] Ziff R M 2009 Explosive growth in biased dynamic percolation on two-dimensional regular lattice networks *Phys. Rev. Lett.* **103** 045701
[5] Scullard C R, Jacobsen J L and Ziff R M 2021 Critical percolation on the Kagome hypergraph *J. Phys. A: Math. Theor.* **54** 055006
[6] Xu J 2017 Time-fractional particle deposition in porous media *J. Phys. A: Math. Theor.* **50** 195002
[7] Ziff R M 2021 Percolation and the pandemic *Physica* A **568** 125723
[8] McMahon T, Chan A, Havlin S and Gallos L K 2022 Spatial correlations in geographical spreading of COVID-19 in the United States. *Sci. Rep.* **12** 699
[9] Thomas J M and Thomas W J 2015 *Principles and Practice of Heterogeneous Catalysis* (New York: Wiley)
[10] van Santen R 2017 *Modern Heterogeneous Catalysis: An Introduction* (New York: Wiley)
[11] Ma Z and Zaera F 2011 Heterogeneous catalysis by metals *Encyclopedia of Inorganic and Bioinorganic Chemistry* (New York: Wiley)
[12] Stamatakis M and Vlachos D G 2012 Unraveling the complexity of catalytic reactions via kinetic Monte Carlo simulation: current status and frontiers *ACS Catal.* **2** 2648–63
[13] Liu D-J, Garcia A, Wang J, Ackerman D M, Wang C-J and Evans J W 2015 Kinetic Monte Carlo simulation of statistical mechanical models and coarse-grained mesoscale descriptions of catalytic reaction–diffusion processes: 1D nanoporous and 2D surface systems *Chem. Rev.* **115** 5979–6050
[14] Zhdanov V P 1991 *Elementary Physicochemical Processes on Solid Surfaces* (New York: Plenum)
[15] Jørgensen M and Grönbeck H 2019 Perspectives on computational catalysis for metal nanoparticles *ACS Catal.* **9** 8872–81

[16] Zhdanov V P and Kasemo B 2000 Simulations of the reaction kinetics on nanometer supported catalyst particles *Surf. Sci. Rep.* **39** 25–104
[17] Unruean P, Plianwong T, Pruksawan S, Kitiyanan B and Ziff R M 2019 Kinetic Monte-Carlo simulation of methane steam reforming over a nickel surface *Catalysts* **9** 946
[18] Nørskov J K, Abild-Pedersen F, Studt F and Bligaard T Density functional theory in surface chemistry and catalysis 2011 *Proc. Natl Acad. Sci. USA* **108** 937–43
[19] Reuter K 2016 *Ab initio* thermodynamics and first-principles microkinetics for surface catalysis *Catal. Lett.* **146** 541–63
[20] Rahmati M, Safdari M-S, Fletcher T H, Argyle M D and Bartholomew C H 2020 Chemical and thermal sintering of supported metals with emphasis on cobalt catalysts during Fischer–Tropsch synthesis *Chem. Rev.* **120** 4455–533
[21] Froment G F 2008 Kinetic modeling of hydrocarbon processing and the effect of catalyst deactivation by coke formation *Catal. Rev.* **50** 1–18
[22] Reshetnikov S I, Petrov R V, Zazhigalov S V and Zagoruiko A N 2020 Mathematical modeling of regeneration of coked Cr–Mg catalyst in fixed bed reactors *Chem. Eng. J.* **380** 122374
[23] Bukowski B C, Keil F J, Ravikovitch P I, Sastre G, Snurr R Q and Coppens M-O 2021 Connecting theory and simulation with experiment for the study of diffusion in nanoporous solids *Adsorption* **27** 683–760
[24] Nepryahin A, Holt E M, Fletcher R S and Rigby S P 2016 Structure-transport relationships in disordered solids using integrated rate of gas sorption and mercury porosimetry *Chem. Eng. Sci.* **152** 663–73
[25] Maris J J E, Fu D, Meirer F and Weckhuysen B M 2021 Single-molecule observation of diffusion and catalysis in nanoporous solids *Adsorption* **27** 423–52
[26] Mishin Y, Herzig C, Bernardini J and Gust W 1997 Grain boundary diffusion: fundamentals to recent developments *Int. Mater. Rev.* **42** 155–78
[27] Thiele E W 1939 Relation between catalytic activity and size of particle *Ind. Eng. Chem.* **31** 916–20
[28] Zavarukhin S G and Rodina V O 2021 Effect of intradiffusion resistance on the chemical process in a nonspherical catalyst pellet *Kinet. Catal.* **62** 551–6
[29] Froment G F 1991 The modeling of catalyst deactivation by coke formation *Catalyst Deactivation* ed C H Bartholomew and J B Butt (Amsterdam: Elsevier) pp 53–83
[30] Mehraban M and Shahraki B H 2019 A mathematical model for decoking process of the catalyst in catalytic naphtha reforming radial flow reactor *Fuel Process. Technol.* **188** 172–8
[31] Zhdanov V P 1993 Application of percolation theory to describing kinetic processes in porous solids *Adv. Catal.* **39** 1–50
[32] Ye G, Wang H, Duan X, Sui Z, Zhou X, Coppens M-O and Yuan W 2019 Pore network modeling of catalyst deactivation by coking, from single site to particle, during propane dehydrogenation *AIChE J.* **65** 140–50
[33] Lin Y, Yang C, Choi C, Zhang W, Machida H and Norinaga K 2021 Lattice Boltzmann simulation of multicomponent reaction–diffusion and coke formation in a catalyst with hierarchical pore structure for dry reforming of methane *Chem. Eng. Sci.* **229** 116105
[34] Lei T, Liu X, Pathak A D, Shetty S, Liu Q and Wen X 2021 Insights into coke formation and removal under operating conditions with a quantum nanoreactor approach *J. Phys. Chem. Lett.* **12** 9413–21
[35] Li H, Yuan X, Gao M, Ye M and Liu Z 2019 Study of catalyst coke distribution based on population balance theory: application to methanol to olefins process *AIChE J.* **65** 1149–61
[36] Ochoa A, Ibarra Á, Bilbao J, Arandes J M and Castaño P 2017 Assessment of thermogravimetric methods for calculating coke combustion-regeneration kinetics of deactivated catalyst *Chem. Eng. Sci.* **171** 459–70
[37] Zhao J, Zhou J, Ye M and Liu Z 2020 Kinetic study on air regeneration of industrial methanol-to-olefin catalyst *Ind. Eng. Chem. Res.* **59** 11953–61
[38] Binder K 1986 Introduction: theory and 'technical' aspects of Monte Carlo simulations *Monte Carlo Methods in Statistical Physics* ed K Binder (Berlin: Springer) pp 1–45
[39] Ziff R M, Gulari E and Barshad Y 1986 Kinetic phase transitions in an irreversible surface-reaction model *Phys. Rev. Lett.* **56** 2553–6
[40] Zhdanov V P, Carlsson P-A and Kasemo B 2008 Kinetics of oxidation of nm-sized soot spherules *Chem. Phys. Lett.* **454** 341–4